ENHANCED MICROMECHANICS OF COMPACTING FIBRE BEDS

Arbabi N.[1], Forghani A.[2], Vaziri R.[1,3], Poursartip, A.[1,2*]
[1] Composites Research Network, Department of Materials Engineering, The University of British Columbia, Vancouver, Canada
[3] Department of Materials Engineering, The University of British Columbia, Vancouver, Canada
[2] Convergent Manufacturing Technologies Inc, Vancouver, Canada
* Corresponding author (anoush.poursartip@ubc.ca)

Keywords: *Processing, Compaction, Fibre Bed*

ABSTRACT

During the processing of unidirectional pre-impregnated composite laminates, an important step is the debulking and compaction of the layers to remove gaps between and within the laminae. During this step, the resin is heated up and can flow relative to the fibre bed. Consequently, the fibre bed elastic properties play a significant role in determining the pressure sharing between the fibre bed and flowing resin, and the shear deformation of the fibre bed. The flow of resin through the fibre bed typically modeled as Darcy flow, and the fibre bed properties of interest include the fibre bed compaction curve, which is a stiffening curve relating the fibre bed normal stress to the normal strain or volume fraction. Although this can be determined experimentally, Cai and Gutowski [1] developed a simple and elegant model based on a network of wavy fibres. This model predicts the transverse through-thickness stiffness E_{33}, which is then used to determine the load sharing between fibre bed and resin at any instant during flow. However, the Gutowski model effectively ignores the fibre bed shear modulus. This is problematic, as although the original models were developed for flat plates, their meaningful use is for predictions for configured structure. Currently, this is done independently of the fibre bed compaction curve by introducing an assumed shear modulus, typically taken to be a constant and back-calculated or fitted to experiments. In this work, we show how a simple modification of the assumed fibre bed representative volume element allows the simultaneous prediction of the full stiffness matrix, with a correlated response between the through-thickness stiffness E_{33} and the shear moduli. This allows for a proper physics and mechanics-based approach to representing all the fibre bed elastic properties coherently.

1 INTRODUCTION

Unidirectional pre-impregnated composite laminates consist of tightly packed fibres that are wavy in general. Any applied load to the prepreg is shared between the fibre bed and the resin. In the early stage of the composite processing, the thermosetting resin is fluid and therefore can flow between the fibres (i.e. through the fibre bed). In an ideal system of perfectly straight fibres, or the case of a very low fibre volume fraction, where there is minimal interaction between fibres, the fibre bed carries insignificant load through-thickness [2]. In reality, the fibres are wavy, and packed at a high volume fraction. The interaction of the tightly packed wavy fibres results in a significant elastic response of the fibre bed that determines the share of pressure that fibres and the resin are carrying. The share of the stress can be stated [2] in an equilibrium equation $\boldsymbol{\sigma} = \boldsymbol{\bar{\sigma}} - \boldsymbol{I}P$ where σ is the effective stress state of the composite, $\bar{\sigma}$ is the effective stress of the fibre bed, I is the identity matrix and P is the resin pressure (compressive is positive). The effective stress of the fibre bed ($\bar{\sigma}$), which is a function of fibre bed deformation, is an important input to flow-compaction models [3]–[8].

The relationship between the effective stress, and the deformation of the fibre bed is determined either experimentally, or theoretically. Springer et al (1983) [9], [10] were among the first ones who explored the flow and compaction of composites during processing. They assumed a sequential compaction model in which the external load is carried by only the resin, and the compaction occurred progressively downward in the laminate layers. Dave et al (1987) [11], [12] and Gutowski (1985) [13] on the other hand considered a squeeze sponge model for the laminate in which the applied pressure is shared between the fibre bed and the resin. Gutowski et al (1987) [14] investigated the relationship between the fibre bed compaction and the stiffness considering the squeeze sponge model. Their experimental work demonstrated that the fibres gradually carry an increasing portion of the applied load. The nonlinearity of the fibre bed compaction curve is a result of the interactions of wavy fibres. Initially, the fibres are wavy, and touching lightly at random points. As the external pressure increases, the fibres straighten, and the number of contact points between them increases. Therefore, the elastic modulus of the fibre bed increases to a point that the general response of the fibre bed is equal to the individual fibres. Smith and Poursartip (1993) [15] compared the sequential and sponge approaches, and concluded that the squeeze sponge model is more accurate in describing the entire compaction process, and the sequential compaction model is a special case of the squeeze sponge model. Later, Hubert and Poursartip (2001) [2] developed an efficient experimental method for direct measurement of the fibre bed compaction curves, which later they used to develop a two-dimensional flow model for the process simulation of complex shape composite laminates [3].

Alongside the experimental approaches to study the fibre bed compaction behavior, attempts were made to predict the fibre bed compaction behavior using analytical models. Focusing on mostly flat panels, and bleed systems, Gutowski et al. (1992) [16], [17] developed an analytical model to describe the response of an aligned, lubricated fibre bundle to the external stress. The three-dimensional model allowed cylindrical modes of elastic dilation and only viscous deformation for the shearing, claiming that the shear deformations are negligible for autoclave processing. Hubert et. al. (1999) [3] used Gutowski's method in combination with soil mechanics problems where the shear response is taken to be elastic to come up with a rate-independent elastic constitutive relation for the fibre bed. Their constitutive model considered the elastic modulus of fibre bed in the direction of the fibres to be a function of the fibre elastic modulus, while the transverse elastic modulus is measured experimentally. The value for the shear modulus is not measured, however they showed the importance of including it for the accurate prediction of deformation of non-flat parts. Later compaction models for the fibre bed either considered the shear modulus of the fibre bed to be zero or a small number just to stabilize the computations[18]–[21].

New processes and complex part geometries require a micromechanical model that is capable of calculating the material properties for all directions, including shear deformation. In this work, we show how a simple modification of the assumed fibre bed representative volume element allows the simultaneous prediction of the full stiffness matrix, with a correlated response between the through-thickness stiffness E_{33} and the shear moduli. This allows for a proper physics and mechanics-based approach to representing all the fibre bed elastic properties coherently.

2 An extended analytical model for fire bed

2.1 Formulation

The formulation of the unit cell developed by Gutowski and Cai [1] is based on a curved beam that is touching at multiple points (Figure 1). The fibres are assumed as curved beams with the following shape:

$$y = \frac{a_0}{2}\left(1 - 2\cos\left(\frac{\pi x}{L}\right)\right) \tag{1}$$

Where a_0 is the height of a curved fibre element, and L is the length of the volume element containing representative fibre (Figure 1).

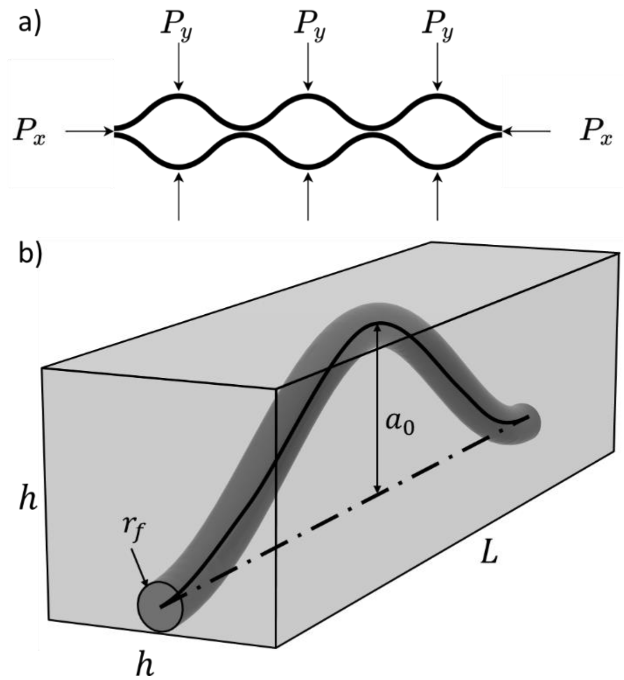

Figure 1: a) Wavy fibres touching each other, and b) a unit cell made of a single fibre in the original Gutowski and Cai model [21]

The unit cell Figure 2b is arranged in a square pattern, which predicts the bulk compression curve based on the volume fraction based on the following formulation:

$$\sigma_b = \frac{3\pi E}{\beta^4} \frac{\left(1 - \sqrt{\frac{V_f}{V_0}}\right)}{\left(\sqrt{\frac{V_a}{V_f}} - 1\right)^4} \tag{2}$$

Where V_f is the fibre volume fraction, V_0 is the initial fibre volume fraction for the unstressed bundle, V_a is the maximum available fibre volume fraction, and $\beta = L/a$ is correlated to fibre waviness. However, this model considers zero shear modulus for the fibre bed, and assumes that the prepreg shear deformation is viscous. This assumption works well for the flat panels and bleed systems, but experimental evidence shows the shear modulus of the prepreg plays a significant role in defining the geometrical accuracy of complex parts, and controlling new processes such as forming and ATL process.

The deformation matrix for compression of a single wavy fibre in the original Gutowski, Cai model is:

$$\begin{Bmatrix} \Delta x \\ \Delta y \end{Bmatrix} = \begin{bmatrix} \frac{a^2 L}{8EI} + \frac{L}{EA} & -\frac{aL^2}{4\pi^2 EI} \\ -\frac{aL^2}{4\pi^2 EI} & \frac{L^3}{192EI} \end{bmatrix} \begin{Bmatrix} P_x \\ P_y \end{Bmatrix} \tag{3}$$

Where Δx is the deformation of the fibres in the fibre direction, and Δy is the deformation in the waviness amplitude direction. We are interested in Δy, and assume that $\Delta x = 0$:

$$0 = \left(\frac{a^2 L}{8EI} + \frac{L}{EA}\right) P_x - \frac{aL^2}{4\pi^2 EI} P_y \tag{4}$$

$$\Delta y = -\frac{aL^2}{4\pi^2 EI} P_x + \frac{L^3}{192EI} P_y \tag{5}$$

Inserting P_x from eq. (4) to eq. (5) we have:

$$\Delta y = -\left(\frac{a^2 L}{8EI} + \frac{L}{EA}\right) + \frac{L^3}{192EI} P_y \tag{6}$$

The two fibres become flatter as they are compressed, thus a changes based on Δy, $a_0 = a + \Delta y$. Since we are interested in compaction in the direction of the waviness, a change in naming $\Delta \mathrm{y} = \mathrm{U}$, and $P_y = P_U$ is considered. It should be mentioned that $\beta = L/a$ is assumed to be constant during compression, similar to the original Gutowski and Cai formulations. The modified formulation becomes:

$$P_U = \frac{I\,\pi^4((a_0 - \mathrm{U})^2 A + 8\,I) E \mathrm{U}}{(a_0 - \mathrm{U})^3 \beta^3 ((a_0 - \mathrm{U})^2 (\pi^4 - 96) A + 8\,I\,\pi^4)} \tag{7}$$

We introduce an angle ψ, to the original curved fibre unit cell to account for the shear modulus of the fibre. The angle ψ in the Extended Fibre bed Model (EFM) is originated from considering the arrangement of the fibres in non-square packing and assumes that the wavy fibres are in touch with this angle. Considering just two fibres, Figure 2b shows the interactions in 2-3 plane, and Figure 2c demonstrates the same interaction looking at the view line. From Figure 2c, $d = a_0 + 2r_f$, where d can be calculated from fibre volume fraction:

$$d = \sqrt{\pi r_f^2 / 2\, V_f cos(\psi) \sin(\psi)} \tag{8}$$

The compaction of two wavy fibres can be modeled using nonlinear springs with a force-deformation behavior derived from the Gutowski and Cai formulation for the compaction of wavy fibres. Using the formula for the force-deformation relation of two fibres from eq. (7), the interaction of the fibres is modeled as nonlinear springs in the 2-3 plane, Figure 2d.

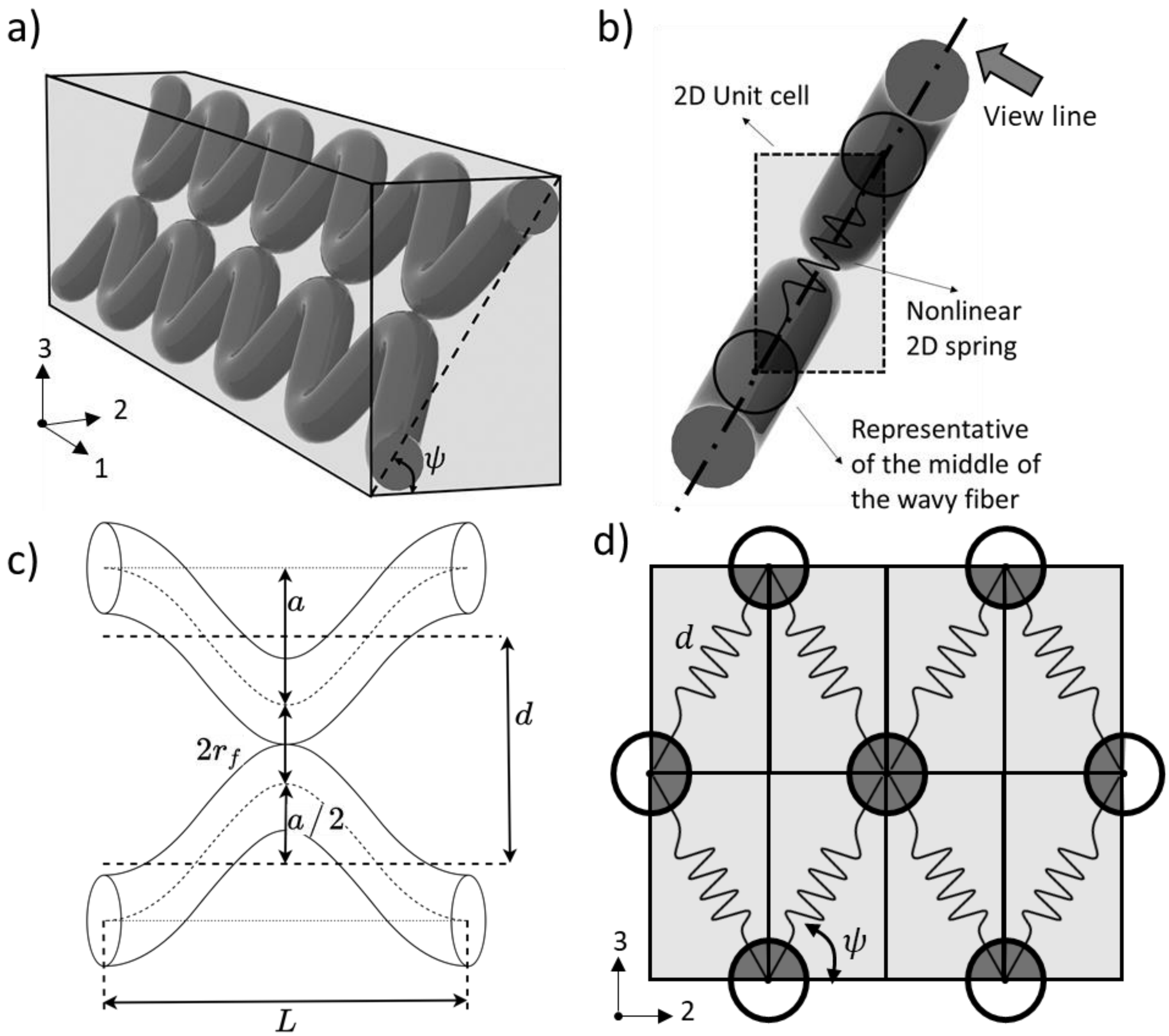

Figure 2: Extended fibre bed model, a) 3D representation, b) 2D unit cell definition, c) fibre interactions and parameters looking at view line, d) representation of the fibre bed microstructure in 2D, modeling the fibre interactions with nonlinear fibres.

2.2 Compaction behavior

In this section, a combination of two unit-cells that form a triangular pattern is considered. Applying a deformation U_c to a triangular unit cell in the original configuration (specified with dashed lines in Figure 3) results in a compressive deformation shown with a solid line in Figure 3.

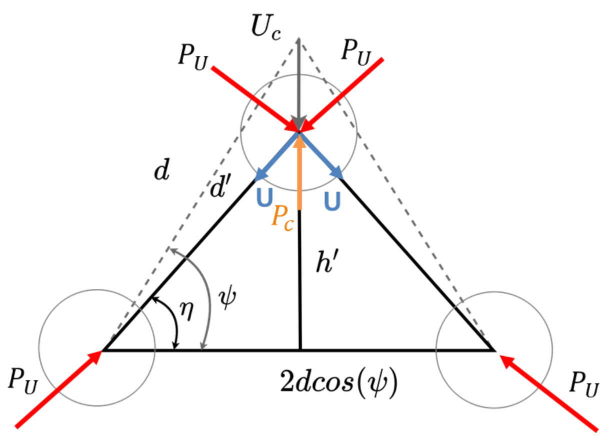

Figure 3: Forces for a triangular unit cell under compression

Applying the compressive deformation U_c, the cell angle after deformation:

$$\eta = \tan^{-1}\left(\frac{sin(\psi)d - U_c}{cos(\psi)d}\right) \tag{9}$$

The deformed cell side is:

$$d' = \frac{dcos(\psi)}{cos(\eta)} \tag{10}$$

The change in the distance between fibres maps to the deformation of the connecting nonlinear spring:

$$U = d - d' = d\left(1 - \frac{cos(\psi)}{cos(\eta)}\right) \tag{11}$$

This deformation is used in eq. (7) to find the corresponding force, P_U. The vertical compression force of the two P_U is equal to $P_c = 2P_U \sin(\eta)$. The derivative of the analytical formula for the compaction pressure with respect to the compaction strain is calculated to determine the evolution of E_{33} modulus.

2.3 Shear Behavior

For calculating the shear modulus of the fibre bed at different compaction levels, two steps of calculation are required. In the first step, a compaction displacement (U_c) is applied to the top of the cell. The new height of the triangle cell is equal to the initial height, minus the applied deformation.

$$h' = \mathrm{d}\sin(\psi) - U_c \tag{12}$$

After the compression step, a shear deformation U_s is applied to the top of the cell. Considering the final deformed configuration shown as a solid line triangle in Figure 4a , the angles for the left side, κ, and the right side, ζ, of the triangle can be calculated as follow:

$$\kappa = \mathrm{atan}\left(\frac{h'}{dcos(\psi) + U_s}\right) \tag{13}$$

$$\zeta = \mathrm{atan}\left(\frac{h'}{dcos(\psi) - U_s}\right) \tag{14}$$

The final length of the connecting springs for the left and right side, a and b can be found as follow:

$$b = \frac{h'}{\sin(\kappa)} = \frac{\mathrm{d}\sin(\psi) - U_c}{\sin(\kappa)} \tag{15}$$

$$c = \frac{h'}{\sin(\zeta)} = \frac{\mathrm{d}\sin(\psi) - U_c}{\sin(\zeta)} \tag{16}$$

Using the deformed lengths, the deformation of each of the springs are:

$$U_b = d - b \tag{17}$$

$$U_c = d - c \tag{18}$$

Substituting eq. (17) and eq. (18) into eq. (7), the forces generated by each of the springs, F_b, and F_c can be calculated. The projection of these forces in the horizontal direction determines the tangential traction force:

$$F_s = F_b\cos(\kappa) - F_c\cos(\zeta) \tag{19}$$

The traction force can be used to calculate the shear modulus of the unit cell:

$$G_{23} = \frac{h' F_s}{2U_s dcos(\psi)} \tag{20}$$

For finding the shear modulus at different levels of compaction, 1% shear deformation is applied following different initial compaction deformation.

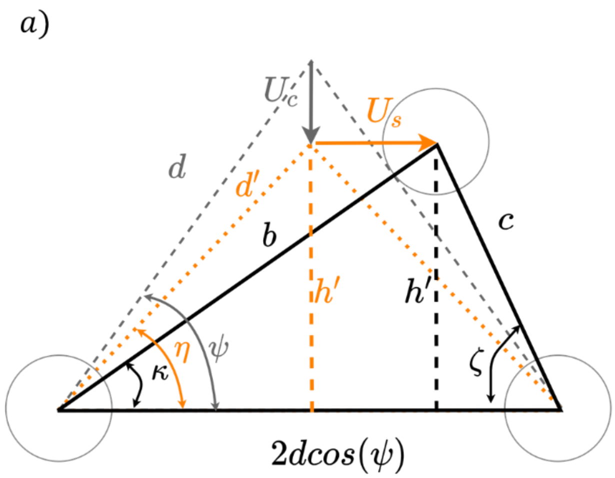

Figure 4: Two steps of applying shear deformation, a) deformations and b) resultant forces

2.4 Results and Discussion:

Considering the T800S/NAT1 prepreg system for this study [22], the initial $V_f = 0.575$, and the fibre radius is $r_f = 2.5\mu m$. Considering the unit cell angle $\psi = 60°$, which results in a uniform hexagonal fibre distribution, the unit cell parameter $d = 6.2\ \mu m$ based on eq. (8), and $a_0 = d - 2r_f = 1.3\mu m$. To determine the effect of volume fraction, a series of compaction deformations are applied to the unit cell, and then the response of the material is measure by small shear/compressive perturbances. At this point, β is the only parameter that is left that can be found by fitting the model to the experiments, however, here the effect of a range of $100 < \beta < 400$ based on the experiments [16], are presented in Figure 5.

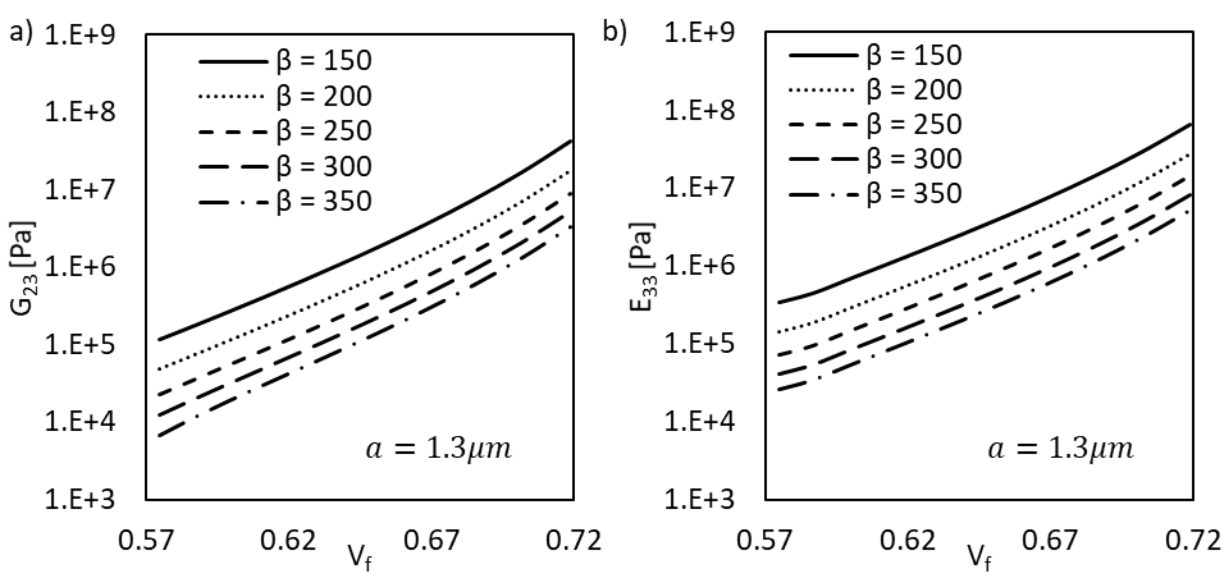

Figure 5: $\boldsymbol{G_{23}}$ and $\boldsymbol{E_{33}}$ based on the Extended Fibre bed Model for different values of β parameter

Figure 5 demonstrates a dependency of the shear and compaction moduli on the fibre volume fraction. Both moduli are increasing exponentially as the fibre bed is compressed. Increasing the value of β while a_0 is constant has an inverse effect on both G_{23} and E_{33}. Given the formula $\beta = L/a$, to increase β while keeping a constant, the value of L should increase. This means that a fibre with constant waviness amplitude now has a longer length. The longer the fibre is, the less leverage it has to withhold applied pressure, thus resulting in lower moduli. This is embedded in eq. (7) where the pressure has an inverse relation with β^3. Since the fibre in the unit cell is rotated along with the fibre axis by $\psi = 60$ the change in the general fibre stiffness, affects both G_{23} and E_{33} simultaneously. The model demonstrates the ability to connect the stiffness matrix components to state variables such as fibre volume fraction as well as providing enough degrees of freedom to adjust the model to the experimental data in follow-on work.

3 Conclusions

Pre-gelation, even though the fibre bed is not very stiff, it plays a big role in the processing behavior of the prepreg material. We have shown that current models do not consider a full stiffness matrix for modeling the fibre bed, primarily by ignoring the shear modulus. A new extended micromechanical model based on Gutowski's original concept of wavy fibres is introduced that allows the simultaneous prediction of the full stiffness matrix, specifically, the compression and shear moduli, during the debulking process. The framework developed in this paper will serve as a basis for further study of the fibre bed behavior during composites processing.

4 REFERENCES

[1] Z. Cai and T. Gutowski, "The 3-D Deformation Behavior of a Lubricated Fiber Bundle," *Journal of Composite Materials*, vol. 26, no. 8, pp. 1207–1237, Aug. 1992, doi: 10.1177/002199839202600808.

[2] P. Hubert and A. Poursartip, "A method for the direct measurement of the fibre bed compaction curve of composite prepregs," *Composites Part A: Applied Science and Manufacturing*, vol. 32, no. 2, pp. 179–187, Feb. 2001, doi: 10.1016/S1359-835X(00)00143-3.

[3] P. Hubert, R. Vaziri, and A. Poursartip, "A two-dimensional flow model for the process simulation of complex shape composite laminates," *International Journal for Numerical Methods in Engineering*, vol. 44, no. 1, pp. 1–26, 1999, doi: https://doi.org/10.1002/(SICI)1097-0207(19990110)44:1<1::AID-NME481>3.0.CO;2-K.

[4] S. M. Haghshenas, R. Vaziri, and A. Poursartip, "Integration of resin flow and stress development in process modelling of composites: Part I – Isotropic formulation," *Journal of Composite Materials*, vol. 52, no. 23, pp. 3137–3155, Sep. 2018, doi: 10.1177/0021998318762295.

[5] S. A. Niaki, A. Forghani, R. Vaziri, and A. Poursartip, "A two-phase integrated flow-stress process model for composites with application to highly compressible phases," *Mechanics of Materials*, vol. 109, pp. 51–66, Jun. 2017, doi: 10.1016/j.mechmat.2017.03.016.

[6] S. A. Niaki, A. Forghani, R. Vaziri, and A. Poursartip, "A three-phase integrated flow-stress model for processing of composites," *Mechanics of Materials*, vol. 117, pp. 152–164, Feb. 2018, doi: 10.1016/j.mechmat.2017.10.012.

[7] S. Amini Niaki, A. Forghani, R. Vaziri, and A. Poursartip, "An Orthotropic Integrated Flow-Stress Model for Process Simulation of Composite Materials—Part I: Two-Phase Systems," *Journal of Manufacturing Science and Engineering*, vol. 141, no. 031010, Jan. 2019, doi: 10.1115/1.4041861.

[8] S. Amini Niaki, "A three-phase integrated flow-stress framework for process modelling of composite materials," 2017.

[9] A. C. Loos and G. S. Springer, "Curing of Epoxy Matrix Composites," *Journal of Composite Materials*, vol. 17, no. 2, pp. 135–169, Mar. 1983, doi: 10.1177/002199838301700204.

[10] G. S. Springer, "Resin Flow During the Cure of Fiber Reinforced Composites," *Journal of Composite Materials*, vol. 16, no. 5, pp. 400–410, Sep. 1982, doi: 10.1177/002199838201600505.

[11] R. Dave, J. L. Kardos, and M. P. Duduković, “A model for resin flow during composite processing: Part 1—general mathematical development,” *Polymer Composites*, vol. 8, no. 1, pp. 29–38, 1987, doi: 10.1002/pc.750080106.

[12] R. Dave, J. L. Kardos, and M. P. Duduković, “A model for resin flow during composite processing part 2: Numerical analysis for unidirectional graphite/epoxy laminates,” *Polymer Composites*, vol. 8, no. 2, pp. 123–132, 1987, doi: 10.1002/pc.750080209.

[13] T. G. Gutowski, “Resin flow/fiber deformation model for composites,” *SAMPE Quarterly*, vol. 16, no. 4, pp. 58–64, 1985.

[14] T. G. Gutowski, Z. Cai, S. Bauer, D. Boucher, J. Kingery, and S. Wineman, “Consolidation Experiments for Laminate Composites,” *Journal of Composite Materials*, vol. 21, no. 7, pp. 650–669, Jul. 1987, doi: 10.1177/002199838702100705.

[15] G. D. Smith and A. Poursartip, “A Comparison of Two Resin Flow Models for Laminate Processing,” *Journal of Composite Materials*, vol. 27, no. 17, pp. 1695–1711, Dec. 1993, doi: 10.1177/002199839302701704.

[16] T. G. Gutowski and G. Dillon, “The Elastic Deformation of Lubricated Carbon Fiber Bundles: Comparison of Theory and Experiments,” *Journal of Composite Materials*, vol. 26, no. 16, pp. 2330–2347, Jan. 1992, doi: 10.1177/002199839202601601.

[17] T. G. Gutowski, T. Morigaki, and Zhong Cai, “The Consolidation of Laminate Composites,” *Journal of Composite Materials*, vol. 21, no. 2, pp. 172–188, Feb. 1987, doi: 10.1177/002199838702100207.

[18] M. Li and C. L. Tucker, “Modeling and simulation of two-dimensional consolidation for thermoset matrix composites,” *Composites Part A: Applied Science and Manufacturing*, vol. 33, no. 6, pp. 877–892, Jun. 2002, doi: 10.1016/S1359-835X(02)00017-9.

[19] Y. Li, M. Li, Z. Zhang, and Y. Gu, “Numerical analysis of parametric effects on consolidation of angle-bended composite laminates,” *Polymer Composites*, vol. 30, no. 10, pp. 1510–1516, 2009, doi: 10.1002/pc.20723.

[20] D. H.-J. A. Lukaszewicz and K. Potter, “Through-thickness compression response of uncured prepreg during manufacture by automated layup,” *Proceedings of the Institution of Mechanical Engineers, Part B: Journal of Engineering Manufacture*, vol. 226, no. 2, pp. 193–202, Feb. 2012, doi: 10.1177/0954405411411817.

[21] J. P.-H. Belnoue, O. J. Nixon-Pearson, D. Ivanov, and S. R. Hallett, “A novel hyper-viscoelastic model for consolidation of toughened prepregs under processing conditions,” *Mechanics of Materials*, vol. 97, pp. 118–134, Jun. 2016, doi: 10.1016/j.mechmat.2016.02.019.

[22] Y. Naito, M. Nishikawa, C. Mobuchon, A. Poursartip, N. Matsuda, and M. Hojo, “Effect of rheological transitions in matrix resin on flow mechanism of carbon Fiber/Epoxy prepreg,” *Composites Part A: Applied Science and Manufacturing*, vol. 151, p. 106612, Dec. 2021, doi: 10.1016/j.compositesa.2021.106612.